Electronic Supplementary Material (ESI) for Soft Matter.

Deciphering the origin of the melting profile of unilamellar phosphatidylcholine liposomes by measuring the turbidity of its suspensions

Petra Maleš[a], Barbara Pem[a], Dražen Petrov[b], Darija Domazet Jurašin[c], Danijela Bakarić[a,] *

[a] Division for Organic Chemistry and Biochemistry, Ruđer Bošković Institute, Bijenička 54, 10000 Zagreb, Croatia

[b] Institute of Molecular Modeling and Simulation, University of Natural Resources and Life Sciences, 1180 Vienna, Austria

[c] Division for Physical Chemistry, Ruđer Bošković Institute, Bijenička 54, 10000 Zagreb, Croatia

Supporting Information

S1. DLS data and microscopic images of LUV and MLV p2

S2. DSC and DLS data of suspensions containing the mixture of MLV and LUV p4

S3. Fitting parameters (MLV and LUV) and residual analysis (LUV) p5

S4. Normalized absorbance difference in MLV: DPPC + 5 % DPPG and DPPC p8

S5. Temperature-dependent lipid bilayer thickness change in LUV p9

S6. Molecular dynamics simulations of lipid bilayers p10

References p16

S1. DLS data and microscopic images of LUV and MLV

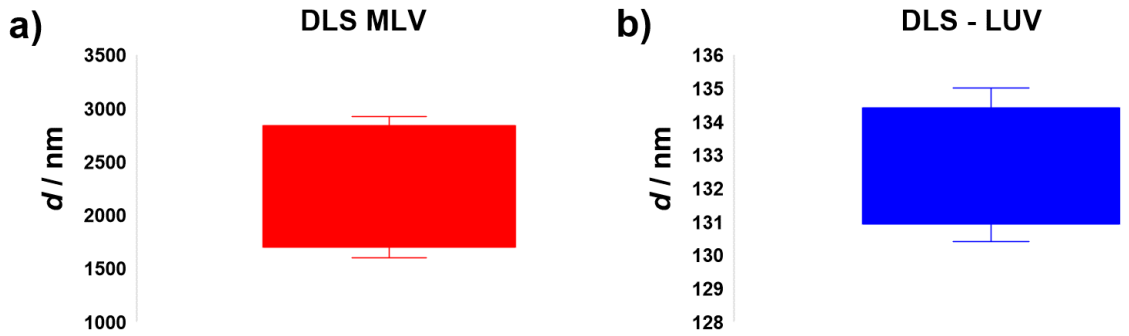

Fig. S1. DLS data of suspensions prepared from DPPC + 5 % DPPG lipids: a) MLV; b) LUV.

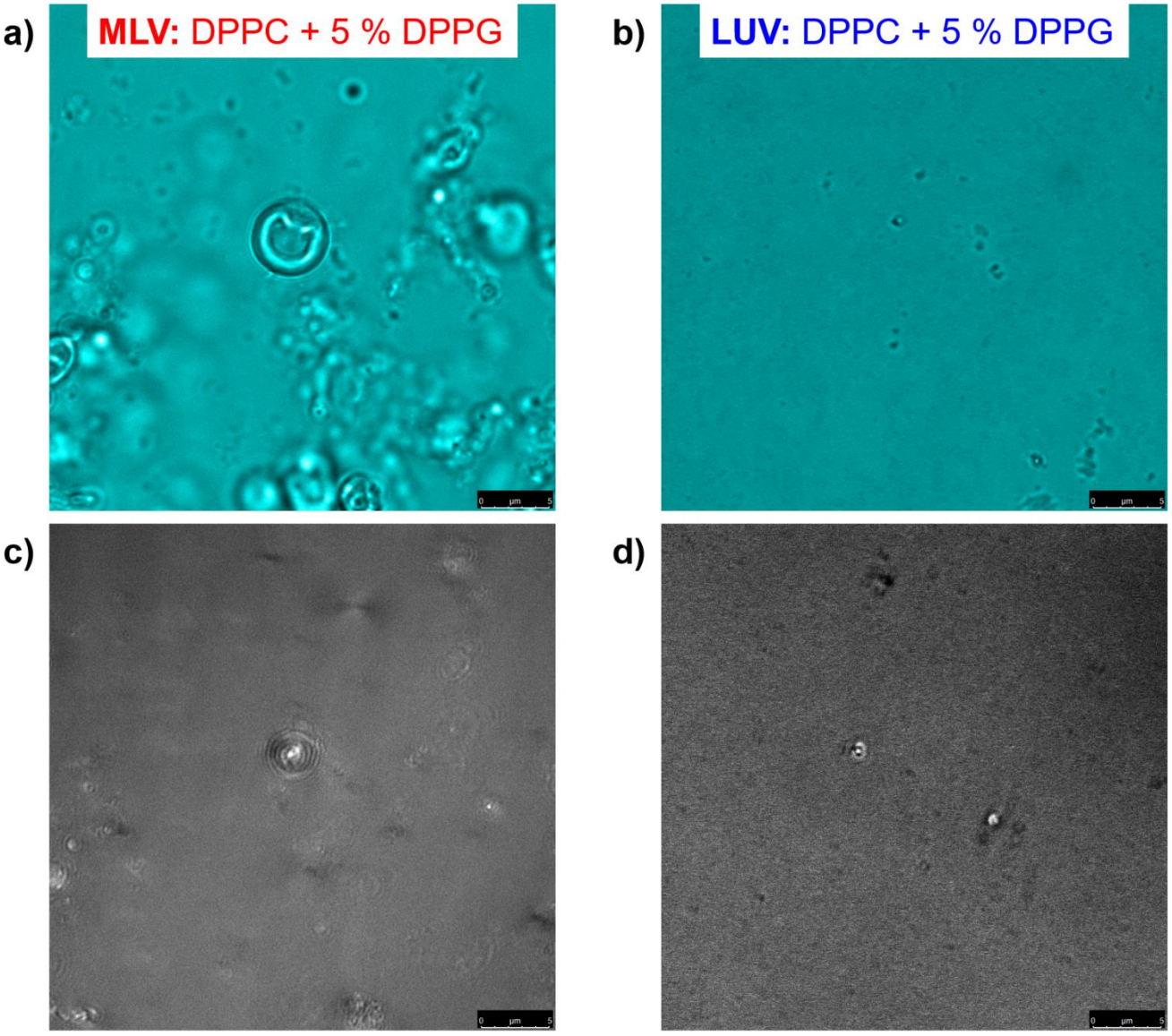

Fig. S2. Confocal microscope images of suspensions prepared from DPPC + 5 % DPPG lipids: a) MLV transmission image; b) LUV transmission image; c) MLV reflection image; d) LUV reflection image.

Although our microscopic images are too low resolution to measure the LUV diameter, from the present images is evident that in the LUV suspension there are only small, very vague granular structures, in contrast to the MLV suspensions in which the observed aggregates are clear and large enough for characterization. If there would be some MLV present in LUV suspension, it would be possible to detect them and to assess their diameter.

S2. DSC and DLS data of suspensions containing the mixture of MLV and LUV

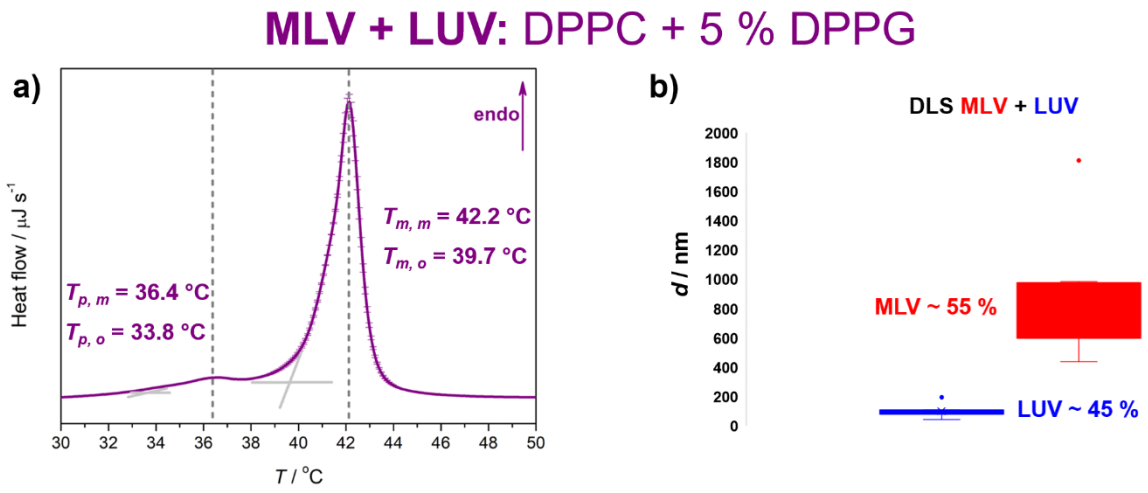

Fig. S3. The data of suspensions prepared from DPPC + 5 % DPPG lipids containing the mixture of MLV and LUV: a) DSC; b) DLS. Phase transition temperatures obtained from the onset and transition maxima are displayed in Fig. S2a.

According to the obtained DSC curves, T_p values coincide with those of MLV, whereas T_m values, as well as the shape of the main phase transition, appear as a combination of MLV and LUV values. These curves, along with DSC curves of MLV and LUV suspension (see the main text, Fig. 2c and Fig. 2d) and literature findings[1,2], support our DLS (and microscopic) data on the absence of MLV in LUV suspension.

S3. Fitting parameters (MLV and LUV) and residual analysis (LUV)

The spectral projections of MLV and LUV obtained by MCA were fitted on double Boltzmann profile (1)

$$y = y_0 + \left(\frac{A_1}{1+e^{\frac{x-x_{01}}{k_1}}} + \frac{A_2}{1+e^{\frac{x-x_{02}}{k_2}}} \right) \quad (1)$$

as well as those obtained from fitting the LUV spectral projections on a single Boltzmann curve

$$y = \frac{A_1 - A_2}{1+e^{\frac{x-x_0}{dx}}} + A_2 \quad (2)$$

A_1 and A_2 in (1) present the "height (depth)" of particular sigmoid transition in expression (1) and the starting (highest) and final (lowest) point obtained by fit in expression (2), respectively; the slopes of particular sigmoid transition are k_1 and k_2 in (1) and dx in (2); the inflection points are x_{01} and x_{02} (T_p and T_m, respectively) in (1) and x_0 in (2), respectively; (Fig. S4, Table S1).

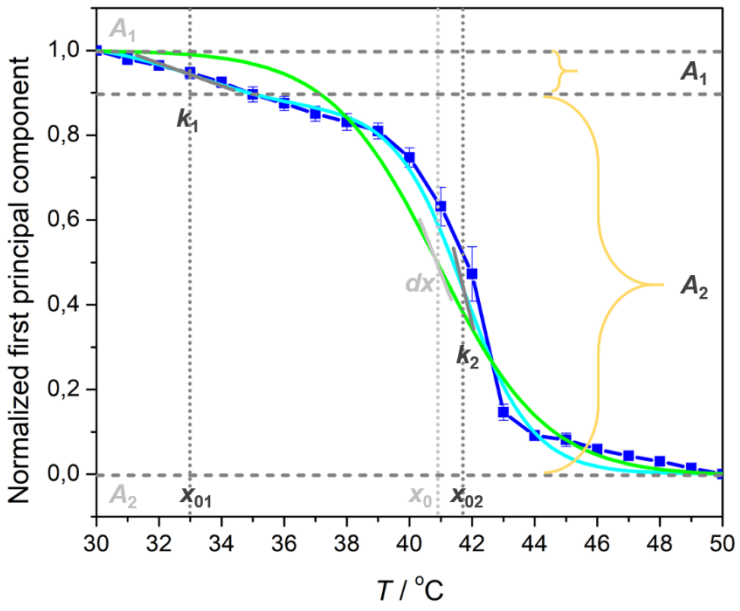

Fig. S4. Normalized first principal component obtained from MCA of LUV in NaCl (I = 100 mM) (blue curve), double Boltzmann fit (cyan curve) and single Boltzmann fit (green curve). Fitting parameters displayed in graph (A_1 and A_2; k_1 and k_2, dx; x_{01} and x_{02}, x_0) are explained in the text above.

Table S1. Parameters obtained from a double (DB) and a single (SB) Boltzmann fit of UV/Vis spectral projections

suspension	Fitting parameters													
	A_1[a]		A_2[a]		k_1[b]	k_2[b]	dx[b]	x_{01}[b]	x_{02}[b]	x_0[b]	R^2		χ^2	
	DB	SB	DB	SB							DB	SB	DB	SB
MLV	0.3	-	0.7	-	1.9 ± 0.4	0.7 ± 0.1	-	34.8 ± 0.7	41.9 ± 0.2	-	0.999	-	3.6	-
LUV	0.1	1	0.9	0	2 ± 2	1.1 ± 0.2	1.7 ± 0.2	33 ± 1	41.7 ± 0.3	40.9 ± 0.2	0.999	0.998	4.4	10.9

[a] Dimensionless quantity; [b] In °C.

Residual analysis obtained from fitting the normalized first principal component on a single and double Boltzmann curve is displayed in Fig. S5.

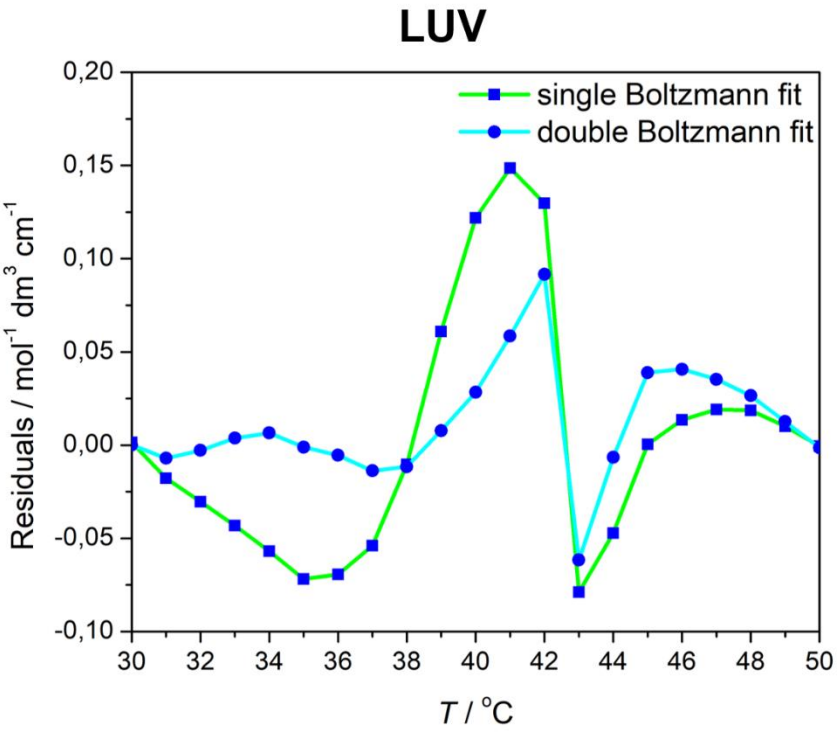

Fig. S5. Residuals obtained from fitting the spectral projections of LUV. Single Boltzmann fit is labeled with green curve with (blue) squares and double Boltzmann fit is labeled with cyan curve with (blue) circles.

S4. Normalized absorbance difference in MLV: DPPC + 5 % DPPG and DPPC

When the temperature-dependent UV/Vis spectra of MLV DPPC (data taken from[3]) are treated in the same way as MLV DPPC + 5 % DPPG (using the relations (6) and (7), the plot in Fig. S6 is obtained.

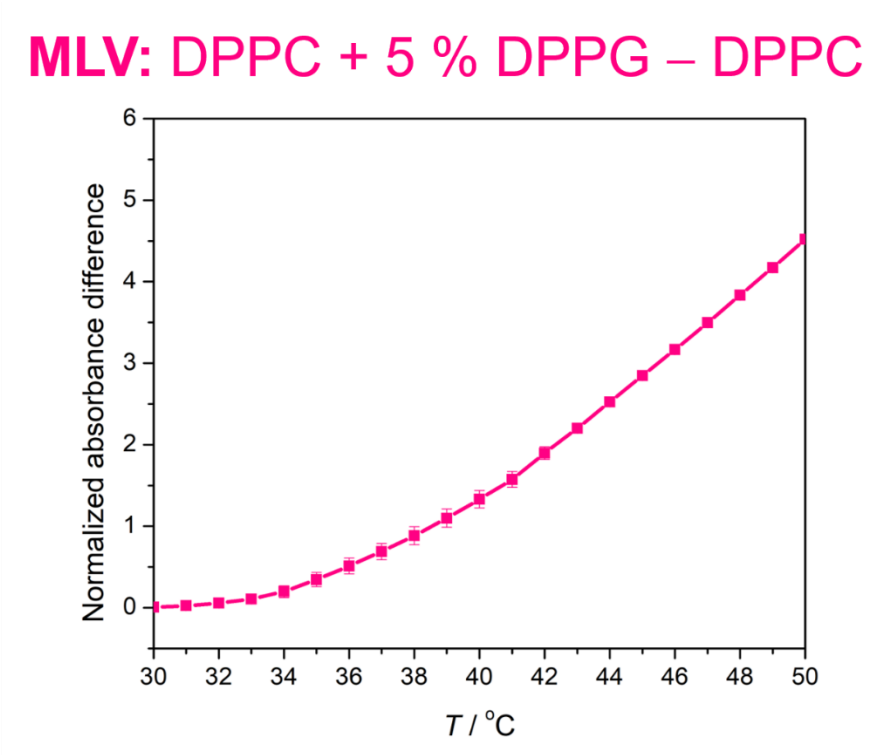

Fig. S6. Normalized absorbance difference (MLV: DPPC + 5 % DPPG – DPPC) in the temperature dependence

According to the Fig. S6, the greatest deviations in temperature-dependent UV/Vis spectra of DPPC MLV, prepared in the absence and in the presence of DPPG, appear above pretransition temperature (~ 34 °C). This findings suggest that the corresponding spectra, no matter of their seemingly resemblance (it seems more appropriate to say that in the absence of chromophore groups UV/Vis spectra of all the compounds look very much alike), they display a fundamental difference due to different scattering cross sections and lipid geometrical features[4]. Additionally, it has to be emphasized that the pretransition in pure DPPC MLV is more cooperative that in DPPC + 5 % DPPG (see [3]). More detail discussion of the observed phenomena is out of the scope of this paper.

S5. Temperature-dependent lipid bilayer thickness change in LUV

Table S2. Temperature-dependent bilayer thickness determined using the HoloPy package and scripts from Wang et al. (2019)[4,5].

T / °C	t/nm
30	7.36 ± 0.04
31	7.35 ± 0.04
32	7.33 ± 0.04
33	7.32 ± 0.04
34	7.30 ± 0.04
35	7.27 ± 0.04
36	7.25 ± 0.04
37	7.23 ± 0.04
38	7.21 ± 0.04
39	7.19 ± 0.04
40	7.14 ± 0.04
41	7.03 ± 0.10
42	6.91 ± 0.10
43	6.61 ± 0.07
44	6.56 ± 0.05
45	6.55 ± 0.05
46	6.53 ± 0.05
47	6.51 ± 0.05
48	6.50 ± 0.05
49	6.50 ± 0.05
50	6.50 ± 0.05

S6. Molecular dynamics simulations of lipid bilayers

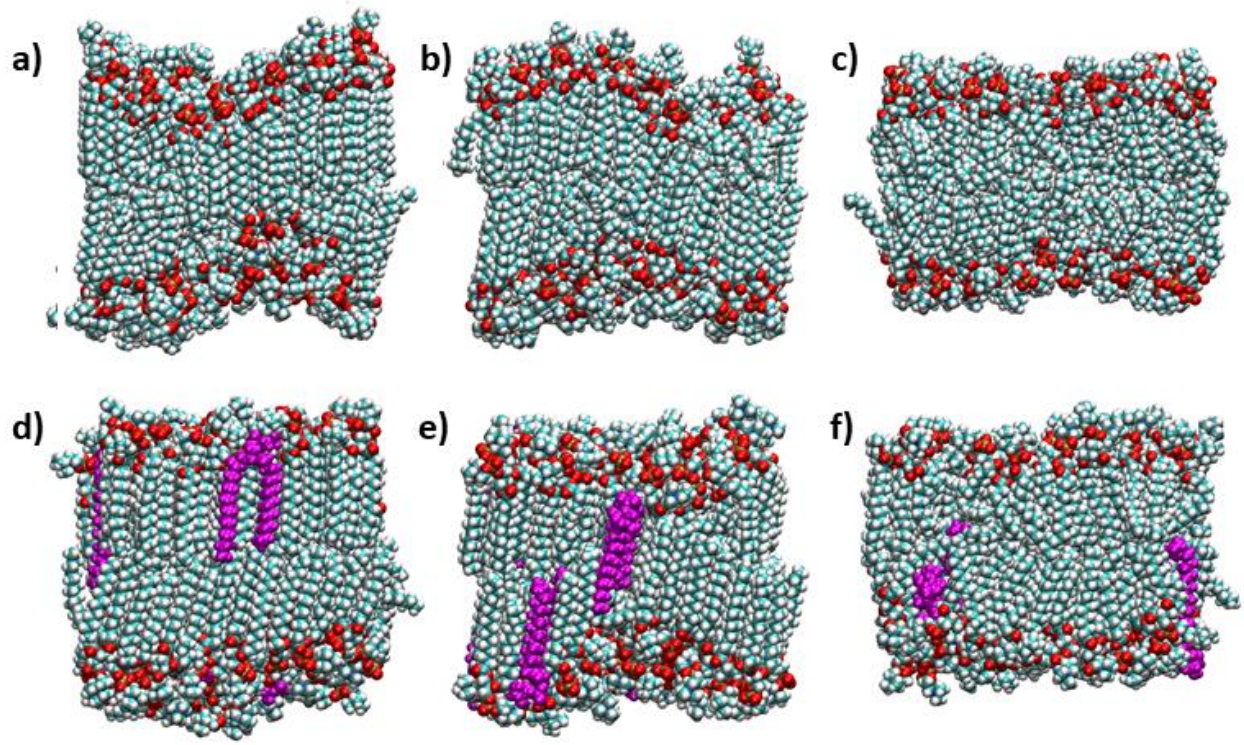

Fig. S7. Snapshots of final frames of MD production runs for a) DPPC bilayers at 30 °C, b) DPPC bilayers at 36 °C, c) DPPC bilayers at 50 °C, d) DPPC + 5% DPPG bilayers at 30 °C, e) DPPC + 5% DPPG bilayers at 36 °C and f) DPPC + 5% DPPG bilayers at 50 °C. All snapshots are generated in VMD. All molecules are represented as their van der Waals radii, and DPPG molecules are colored in magenta for emphasis.

The Fig. S7 shows the structure of each membrane after 100 ns of simulation. The difference between gel ($L_{\beta'}$) and fluid (L_{α}) phase can be seen clearly in the arrangement of acyl chains and membrane thickness.

Deuterium order parameters for carbon atoms of acyl chains are displayed in Fig. S8.

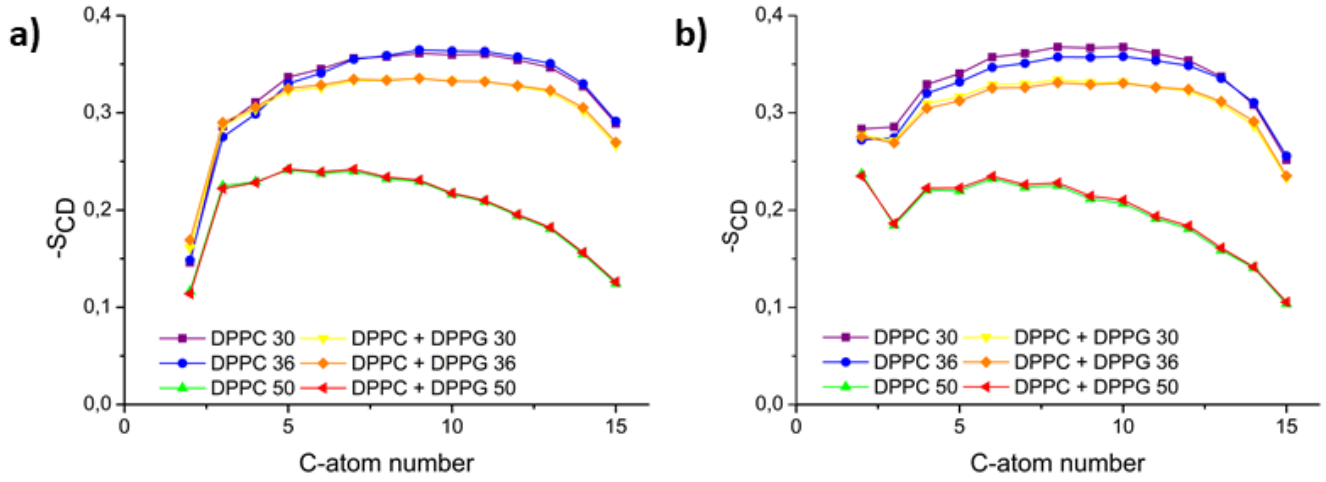

Fig. S8. Deuterium order parameters for carbon atoms in DPPC and DPPG acyl chains: a) chain 1 (corresponding to atoms C21-C216) and b) chain 2 (corresponding to atoms C31-C316).

Area per lipid (APL) and membrane thickness at different temperatures are displayed in Table S3.
Table S3. Area per lipid (APL) and membrane thickness calculated by two methods for DPPC and DPPC + 5% DPPG systems at different temperatures.

System	Temperature (°C)	APL (nm^2)	*Membrane thickness (nm)*	
			As P – P distance	*From water density profiles*
DPPC	30	0.51 ± 0.02	4.82	6.20
	36	0.52 ± 0.01	4.68	6.04
	50	0.60 ± 0.02	4.00	5.21
DPPC + 5% DPPG	30	0.50 ± 0.01	4.93	6.20
	36	0.50 ± 0.01	4.81	6.19
	50	0.60 ± 0.02	4.06	5.42

Partial mass density profiles were obtained by GROMACS module *gmx density*, and show the mass density of lipid components, as well as water, across the z-axis of the simulation box. DPPC headgroups consisted of atoms P, O11-O14, N and C11-C15 (as labeled in Fig. 1 of the main text), DPPG headgroups consisted of P, O11-O14, C11-C13, OC2 and OC3, glycerol ester group encompassed C1-C3, O21, C21, O22, O31, C31 and O32, and the rest was treated as acyl chains.

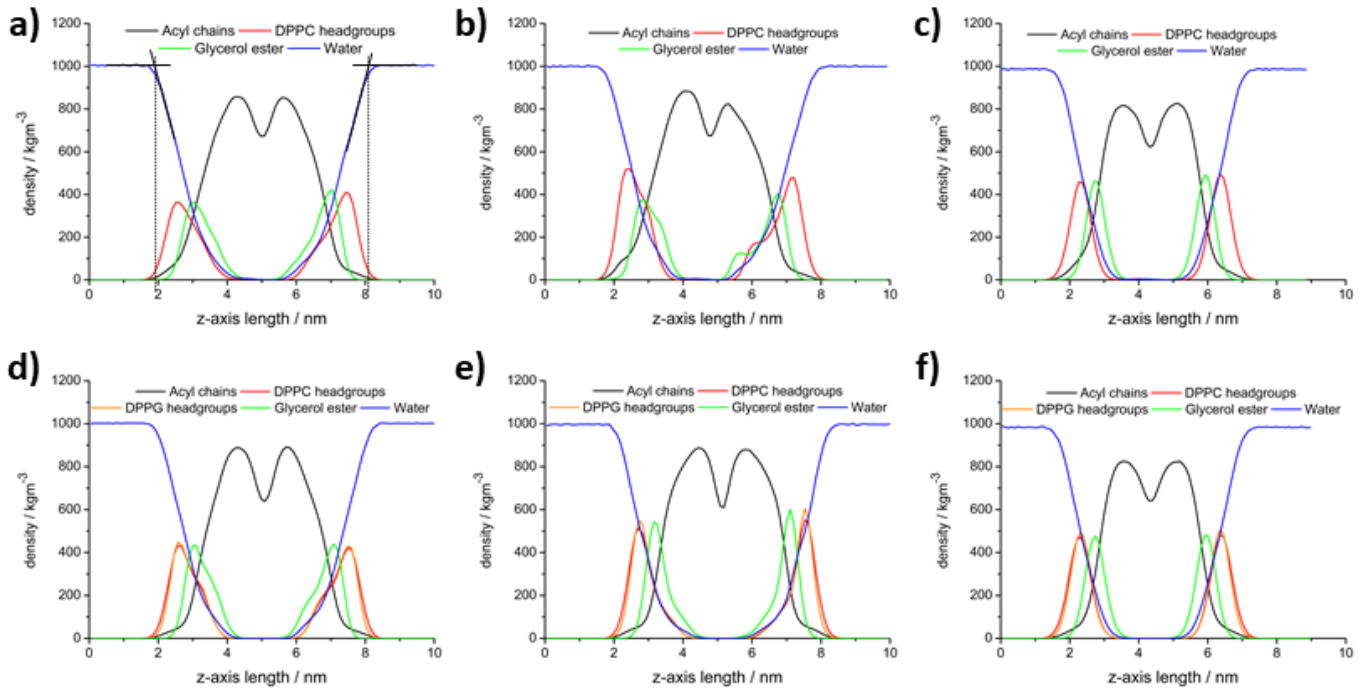

Fig. S9. Partial density profiles for DPPC and DPPG acyl chains, headgroups, glycerol ester fragment, and water molecules: a) DPPC bilayers at 30 °C, b) DPPC bilayers at 36 °C, c) DPPC bilayers at 50 °C, d) DPPC + 5% DPPG bilayers at 30 °C, e) DPPC + 5% DPPG bilayers at 36 °C and f) DPPC + 5% DPPG bilayers at 50 °C. The dotted line in graph a) represents the limit used for calculating bilayer thicknesses.

As seen in Fig. S9, the profiles are mostly symmetrical, with the exception of membranes at 36 °C, where the asymmetry between upper and lower leaflets likely stems from the rippling. The profiles for lipid components differ in shape at different temperatures. In $L_{\beta'}$ phase, the acyl chain profiles are wider at the base with narrower peaks, indicating tighter packing and higher bilayer thickness. The headgroup profiles are extended towards the acyl chains, showing that some of the headgroups are inserted closer to the membrane center. At L_{α} phase membranes are narrower with normally distributed peaks of acyl chains and headgroups, since the entire membrane is uniform. Density profiles also show there is a higher density of water surrounding lipid headgroups compared to the glycerol ester region, and there is even some water penetrating the acyl chain region, as was observed in literature.[6]

Hydrogen bonding patterns (Table S4) were determined using the H-bond analysis module in VMD, by sampling 20 frames of production runs. Patterns are labeled according to the number of H-bonds one water molecule forms with one unique lipid molecule: pattern 1 stands for one bond with only one lipid, pattern 2 is two bonds with the same lipid, pattern 11 means one bond with two lipid molecules each, and pattern 21 means 2 bonds with one lipid and one bond with another. All other patterns were not observed in significant amounts in any of the simulations.

Table S4. Hydrogen bonding patterns between water molecules and DPPC/DPPG for studied systems DPPC (+ 5 % DPPG) at simulated temperatures (30 °C, 36 °C, 50 °C).

System	**Bonding pattern**			
	1	**2**	**11**	**21**
DPPC 30 °C	81 ± 2%	2 ± 2%	15 ± 2%	0.4 ± 0.3%
DPPC 36 °C	81 ± 2%	4 ± 1%	14 ± 2%	0.4 ± 0.2%
DPPC 50 °C	84 ± 1%	4 ± 1%	12 ± 1%	0.2 ± 0.2%
DPPC + 5 % DPPG 30 °C	82 ± 2%	3 ± 1%	14 ± 2%	0.5 ± 0.3%
DPPC + 5 % DPPG 36 °C	81 ± 2%	4 ± 1%	15 ± 1%	0.3 ± 0.3%
DPPC + % % DPPG 50 °C	86 ± 1%	4 ± 1%	10 ± 1%	0.3 ± 0.3%

Details on radial distribution functions not included in the main text are presented in Fig. S10 and Table S5.

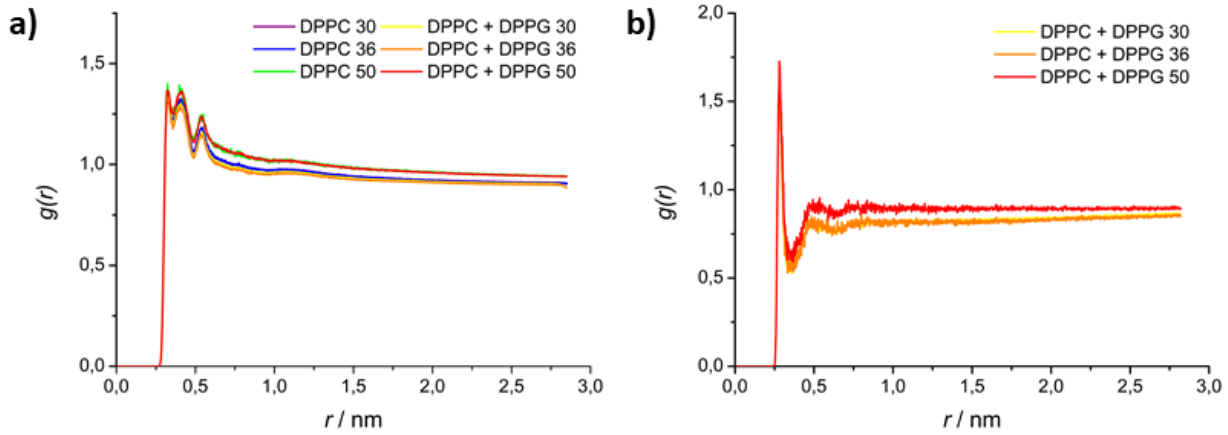

Fig. S10. Radial distribution functions of a) water oxygen with trimethyl-amino group as reference; b) water oxygen with DPPG hydroxyl groups (O_H) as reference.

In Fig. S10.a) the presence of three close peaks is the result of three separate methyl groups in close contact with water. Fig. S10.b) shows two peaks, indicating two hydration shells around DPPG hydroxyl groups.

Table S5. Cumulative number radial distribution functions of water oxygen with select lipid atoms as references, for studied systems DPPC (+ 5 % DPPG) at simulated temperatures (30 °C, 36 °C, 50 °C).

System	**Cumulative number RDF**				
	P-O_{wat}	**N-O_{wat}**	**O_P-O_{wat}**	**O_C-O_{wat}**	**O_H-O_{wat}**
DPPC 30 °C	5.88	16.77	2.41	0.99	n.a.
DPPC 36 °C	5.87	16.68	2.42	0.99	n.a.
DPPC 50 °C	6.02	16.87	2.49	1.09	n.a.
DPPC + 5 % DPPG 30 °C	5.79	16.51	2.39	0.95	1.70
DPPC + 5 % DPPG 36 °C	5.72	16.28	2.37	0.94	1.75
DPPC + % % DPPG 50 °C	6.04	16.86	2.50	1.10	1.88

n.a. = not applicable

Cumulative number RDF values indicate the average number of atoms within a certain radius *r* of the reference atom or group. The radius *r* used to obtain the average number of water molecules

in the hydration shells of each atom or group was taken from the position of first minimum of their respective RDF, which corresponds to the edge of the hydration shell.

DPPG has much larger maximum at cos θ = −0.61 compared to DPPC, but no plateau region. Thus, DPPG is more likely to draw both water oxygens and hydrogens towards itself, while DPPC prefers interacting with the water hydrogen only (Fig. S11).

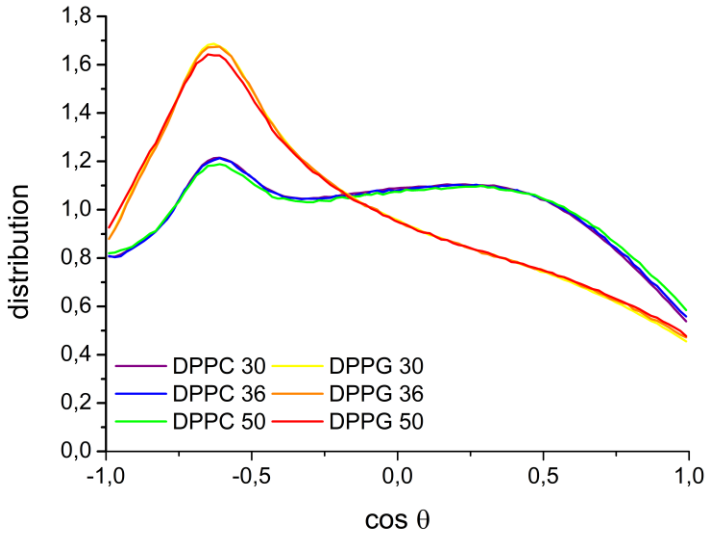

Fig. S11. Angular distribution functions for water separately around DPPC and DPPG headgroups.

References:

1 T. Heimburg, *Biochim. Biophys. Acta - Biomembr.*, 1998, **1415**, 147–162.

2 H. Ebel, P. Grabitz and T. Heimburg, *J. Phys. Chem. B*, 2001, **105**, 7353–7360.

3 P. Maleš, Z. Brkljača, D. Domazet Jurašin and D. Bakarić, *Spectrochim. Acta Part A Mol. Biomol. Spectrosc.*, 2022, **272**, 121013.

4 A. Wang, C. Chan Miller and J. W. Szostak, *Biophys. J.*, 2019, **116**, 659–669.

5 https://github.com/anna-wang/vesicle-turbidity, (accessed 27.6.2022).

6 T. Zaraiskaya and K. R. Jeffrey, *Biophys. J.*, 2005, **88**, 4017–4031.